Heterogeneous Catalysis

International Edition: DOI: 10.1002/anie.201904883
German Edition: DOI: 10.1002/ange.201904883

Pentacoordinated Al^{3+}-Stabilized Active Pd Structures on Al_2O_3-Coated Palladium Catalysts for Methane Combustion

Huimei Duan[+], Rui You[+], Shutao Xu, Zhaorui Li, Kun Qian, Tian Cao, Weixin Huang, and Xinhe Bao*

Abstract: *Supported Pd catalysts are active in catalyzing the highly exothermic methane combustion reaction but tend to be deactivated owing to local hyperthermal environments. Herein we report an effective approach to stabilize Pd/SiO_2 catalysts with porous Al_2O_3 overlayers coated by atomic layer deposition (ALD). ^{27}Al magic angle spinning NMR analysis showed that Al_2O_3 overlayers on Pd particles coated by the ALD method are rich in pentacoordinated Al^{3+} sites capable of strongly interacting with adjacent surface PdO_x phases on supported Pd particles. Consequently, Al_2O_3-decorated Pd/SiO_2 catalysts exhibit active and stable PdO_x and Pd–PdO_x structures to efficiently catalyze methane combustion between 200 and 850 °C. These results reveal the unique structural characteristics of Al_2O_3 overlayers on metal surfaces coated by the ALD method and provide a practical strategy to explore stable and efficient supported Pd catalysts for methane combustion.*

The elimination of methane exhausts from natural-gas-powered applications is an urgent environmental issue of much concern owing to the high greenhouse effect of methane.[1] Palladium-based catalysts have been extensively investigated for catalytic methane combustion, and this catalytic reaction is structure-sensitive.[1b,2] Both experimental and DFT calculation studies suggest the Pd–PdO_x interface as the most catalytically active structure in dissociating CH_4, the rate-determining step in methane combustion, because OH formation at a PdO_x site promotes CH_4 decomposition at a neighboring Pd site.[3] However, the Pd–PdO_x interface is always metastable on supported Pd catalysts during the highly exothermic methane combustion reaction owing to the facile decomposition of PdO_x species at high temperatures.[4] The decomposition of PdO_x species into less active Pd species also causes a serious practical problem for the catalytic combustion of methane from vehicle exhausts, whose temperature rises and falls frequently and quickly owing to the polytropic operating conditions as vehicles move. Therefore, the metallic Pd phase must be able to undergo fast reoxidation to recover the active PdO_x phase and ensure the catalytic efficiency as the temperature falls quickly. An effective strategy to fabricate stable and efficient supported Pd catalysts for methane combustion is to form supported Pd (core)@active oxide (shell) catalysts.[5,6] On one hand, the oxide shells protect Pd cores from sintering. On the other hand, the introduction of a palladium–active oxide interface improves the catalytic activity of metallic Pd particles in methane combustion.

The coating of thickness-controlled Al_2O_3 overlayers on metal particles by atomic layer deposition (ALD) has been demonstrated as a novel powerful strategy to prepare sintering-resistant supported metal catalysts.[7] However, the underlying mechanism for the much-enhanced stabilizing effect of ALD Al_2O_3 overlayers on metal particles over the widely used Al_2O_3 supports remains unknown. Herein, we report the effect of ALD Al_2O_3 overlayers on the stability and catalytic performance of supported Pd catalysts for the methane combustion reaction. Our results reveal that ALD Al_2O_3 overlayers on Pd particles are rich in pentacoordinated Al^{3+} sites capable of strongly interacting with adjacent surface PdO_x phases to form stable PdO_x and Pd–PdO_x structures, leading to high and stable activity in catalyzing the methane combustion reaction.

To minimize the interference of different structures of Pd particles, uniformly sized Pd cubes and octahedra supported on as-synthesized SiO_2 nanospheres (size: 410–450 nm, see Figure S1 in the Supporting Information; BET specific surface area: 14.9 $m^2 g^{-1}$, see Table S1 in the Supporting Information) were adopted as the starting supported Pd catalysts. TEM and high-resolution TEM (HRTEM) images (see Figure S2) showed that cubic Pd (c-Pd) and octahedral Pd (o-Pd) nanocrystals (NCs) enclosed with {100} and {111} facets, respectively, are uniform and have similar sizes of approximately 7.0 nm, in agreement with previous results.[8] The morphologies of c-Pd and o-Pd NCs were largely maintained in the c-Pd/SiO_2 and o-Pd/SiO_2 catalysts, as demonstrated by their representative TEM and HRTEM images (see Figure S2). Thus, the nucleation and growth behaviors of Pd nanocrystals seemed not affected much by the presence of SiO_2 in the synthetic approach, which could be associated with the relative inertness of the SiO_2 surface. The BET specific surface areas of the Pd/SiO_2 catalysts were

[*] H. Duan,[+] Dr. R. You,[+] Z. Li, Dr. K. Qian, Dr. T. Cao, Prof. Dr. W. Huang, Prof. Dr. X. Bao
Hefei National Laboratory for Physical Sciences at the Microscale
Key Laboratory of Surface and Interface Chemistry and Energy Catalysis of Anhui Higher Education Institutes, CAS Key Laboratory of Materials for Energy Conversion and Department of Chemical Physics, University of Science and Technology of China
Jinzhai Road 96, Hefei 230026 (P. R. China)
E-mail: huangwx@ustc.edu.cn
Prof. Dr. S. Xu, Prof. Dr. X. Bao
State Key of Laboratory of Catalysis
Dalian Institute of Chemical Physics, Chinese Academy of Sciences
Zhongshan Road 457, Dalian 116023 (P. R. China)
[+] These authors contributed equally to this work.
Supporting information and the ORCID identification number(s) for the author(s) of this article can be found under: https://doi.org/10.1002/anie.201904883.

similar to that of SiO_2 (see Table S1). The XRD patterns only detected the diffraction patterns arising from the metallic Pd phase, whereas XPS spectra showed the Pd $3d_{5/2}$ binding energies of metallic Pd and PdO_x species (see Figure S3), thus indicating the surface oxidation of supported Pd NCs.

The Pd/SiO_2 catalysts were coated with Al_2O_3 overlayers in 40 cycles of ALD. The resulting $Al_2O_3/Pd/SiO_2$ catalysts were characterized by TEM, HAADF-STEM, and energy dispersive spectroscopy (EDS) elemental mapping (Figure 1; see also Figures S4 and S5). Al_2O_3 overlayers with a thickness of approximately 8 nm were clearly identified in the edge

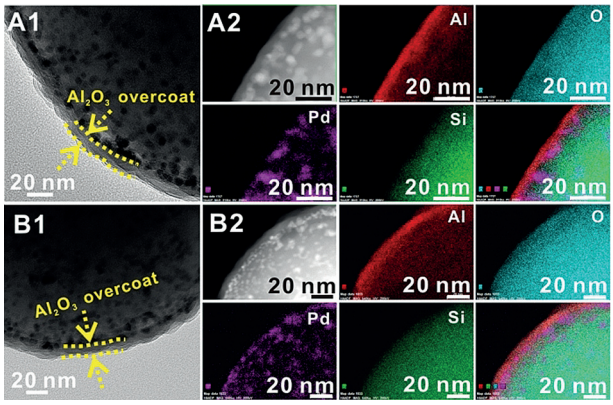

Figure 1. TEM images, HAADF-STEM images, and EDS elemental mapping images of Al_2O_3/c-Pd/SiO_2 (A1, A2)) and Al_2O_3/o-Pd/SiO_2 (B1, B2).

regions in the TEM images, thus indicating an average Al_2O_3 growth rate of approximately 2 Å per ALD cycle. The reported ideal Al_2O_3 ALD growth rates measured on flat substrates are typically 1.1–1.3 Å per ALD cycle.[7a,9] However, higher growth rates were often observed for Al_2O_3 ALD growth on particles,[7b,10] which was proposed to arise from the different H_2O adsorption/desorption kinetics on particles as compared to flat substrates.[10a,c] It was also observed that exposure to a large amount of H_2O in the Al_2O_3 ALD growth procedure as in our case could result in a strongly hydroxylated ALD Al_2O_3 surface and a large growth rate.[10a] Both EDS elemental mapping images and EDS elemental line scan profiles demonstrate distributions of Al_2O_3 overlayers across the whole of the Pd/SiO_2 catalysts. The BET specific surface areas of the $Al_2O_3/Pd/SiO_2$ catalysts are smaller than those of the corresponding Pd/SiO_2 catalysts, most likely owing to the formation of dense Al_2O_3 overlayers (see Table S1). XRD and Pd 3d XPS characterization results show that the Al_2O_3 overlayers do not influence the Pd speciation of the original Pd/SiO_2 catalysts (see Figure S3).

The dense Al_2O_3 overlayers in $Al_2O_3/Pd/SiO_2$ catalysts completely block the Pd surfaces, and the catalysts barely show CO adsorption or catalytic activity in methane combustion. Thermal treatment can introduce pores within Al_2O_3 overlayers that make embedded Pd particles accessible to reactants.[7] The procedure was optimized as a calcination at 900 °C in 10 % O_2/Ar for 6 h, followed by reduction at 300 °C in 5 % H_2/Ar for 45 min (see Figure S6). The acquired catalysts are denoted as $Al_2O_3/Pd/SiO_2$-T. CO pulse chemisorption results (see Figure S7 and Table S2) evidence CO adsorption on $Al_2O_3/Pd/SiO_2$-T in decreased amounts as compared to Pd/SiO_2-T (see Figure S8 for TEM and HRTEM images of Pd/SiO_2-T (Pd loading: 7.48 and 5.67 wt %) and $Al_2O_3/Pd/SiO_2$-T catalysts (Pd loading: 7.30 and 5.53 wt %)). Severe aggregation of Pd nanocrystals occurred during thermal treatment of Pd/SiO_2, but not $Al_2O_3/Pd/SiO_2$. Thus, the Al_2O_3 overlayers can effectively prevent Pd particles from sintering up to 900 °C. The BET specific surface areas of SiO_2-T and Pd/SiO_2-T catalysts were slightly smaller than those of corresponding SiO_2 and Pd/SiO_2 catalysts owing to sintering (see Table S1), whereas the BET specific surface areas of $Al_2O_3/Pd/SiO_2$-T catalysts were slightly larger than those of the corresponding $Al_2O_3/Pd/SiO_2$ catalysts, a result consistent with the creation of pores within Al_2O_3 overlayers of $Al_2O_3/Pd/SiO_2$-T catalysts.

Pd/SiO_2-T and $Al_2O_3/Pd/SiO_2$-T catalysts displayed the diffraction pattern of the metallic Pd phase in their XRD patterns (Figure 2 A) and the Pd $3d_{5/2}$ binding energies of metallic Pd and PdO_x species, at 335.3 and 336.8 eV, respectively,[11] in their Pd 3d XPS spectra (Figure 2 B). The PdO_x species should result from surface oxidation of Pd particles exposed to ambient atmosphere. Metallic Pd dominated on the surface of all the catalysts, and the PdO_x:Pd XPS ratios were higher on $Al_2O_3/Pd/SiO_2$-T catalysts than the corresponding Pd/SiO_2-T catalysts (see Table S3). DRIFT spectra of CO chemisorption on Pd/SiO_2-T showed dominant vibrational bands below 2100 cm^{-1} and a very weak band at 2170 cm^{-1} arising from CO bridge-adsorbed at Pd^0 and linearly adsorbed at Pd^{II} sites, respectively.[12] More specifically, the vibrational bands at 1985/1972 and 1946/1935 cm^{-1} represent CO adsorbed at step/edge and terrace sites of Pd particles, respectively.[12a–f] Both the vibrational-band inten-

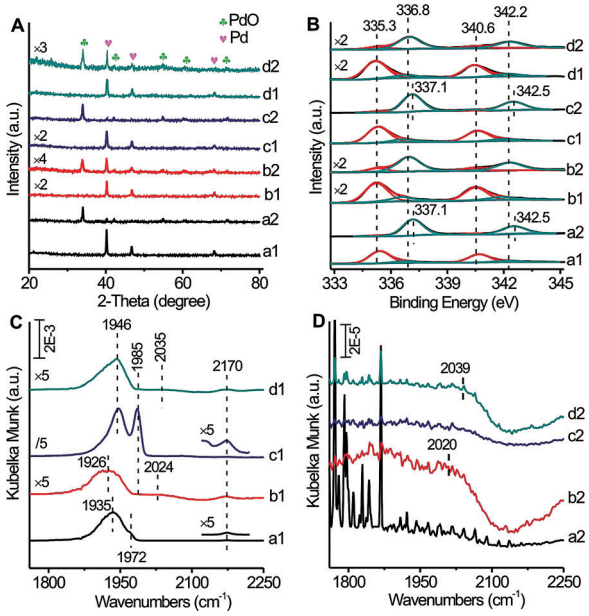

Figure 2. A) XRD patterns, B) Pd 3d XPS spectra, and C, D) DRIFT spectra of saturated CO chemisorption at 30 °C of c-Pd/SiO_2-T (a1, a2), Al_2O_3/c-Pd/SiO_2-T (b1, b2), o-Pd/SiO_2-T (c1, c2), and Al_2O_3/o-Pd/SiO_2-T (d1, d2) before and after activity evaluations in methane combustion.

sity and density of step/edge sites of o-Pd/SiO_2-T are much higher than those of c-Pd/SiO_2-T, thus suggesting very different surface structures of the Pd particles in both catalysts, although they were subjected to harsh calcination treatment at 900 °C followed by reduction at 300 °C. This difference should be related to the original octahedral and cubic Pd nanocrystals, respectively, in o-Pd/SiO_2-T and c-Pd/SiO_2-T, and implies the influence of the original surface structures of the catalyst particles on the reconstructed surface structures, consistent with previous reports.[13]

After the decoration of Al_2O_3 overlayers, the CO vibrational bands at Pd^0 sites were greatly weakened, and those at 1985/1972 cm^{-1} disappeared. This result suggests the preferential deposition of Al_2O_3 overlayers at the step/edge of Pd particles by the ALD method, in agreement with previous observations.[7b, 12b,g] The very weak band of CO adsorbed at Pd^{II} at 2170 cm^{-1} is visible for Al_2O_3/Pd/SiO_2-T catalysts, and the intensity ratio between CO adsorbed at Pd^{II} and CO adsorbed at Pd^0 of Al_2O_3/Pd/SiO_2-T is higher than that of Pd/SiO_2-T, thus suggesting higher fractions of Pd^{II} species on Pd particles in Al_2O_3/Pd/SiO_2-T, which is consistent with the above XPS results. A new but weak vibrational band at 2035/2024 cm^{-1} emerged for Al_2O_3/Pd/SiO_2-T catalysts and corresponds to linearly adsorbed CO at a Pd site interacting with an electron-donor center,[14a,b] which can be attributed to Pd sites at Pd–PdO_x interfaces, since Pd/Al_2O_3 catalysts do not exhibit such a feature of adsorbed CO.[14c,d] These results suggest that Pd–PdO_x interfaces are much more abundant in Al_2O_3/Pd/SiO_2-T catalysts than in Pd/SiO_2-T catalysts, and that the Al_2O_3 overlayers can promote the formation of surface PdO_x species on Pd particles in the fresh catalysts.

The catalytic performance of Pd/SiO_2-T and Al_2O_3/Pd/SiO_2-T catalysts was evaluated in successive cycles of methane combustion between 200 and 850 °C (Figure 3; see also Figures S9–S12). As in previous studies,[4] Pd/SiO_2-T was not stable under the harsh reaction conditions. The CH_4 conversion decreased with each evaluation cycle, and serious deactivation occurred during the cooling ramp of each evaluation cycle. However, Al_2O_3/Pd/SiO_2-T catalysts were very stable. The CH_4 conversion did not change in different evaluation cycles, and only slight deactivation was observed during the cooling ramp for the Al_2O_3/c-Pd/SiO_2-T catalyst,

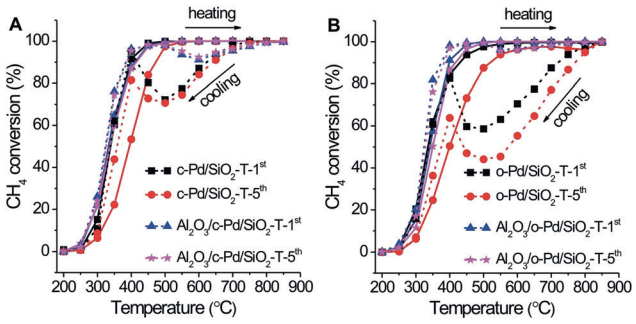

Figure 3. Methane light-off curves as a function of reaction temperature of various A) c-Pd/SiO_2-T and B) o-Pd/SiO_2-T catalysts during successive heating (solid lines) and cooling ramps (dashed lines) up to five cycles.

whereas no deactivation was observed for the Al_2O_3/o-Pd/SiO_2-T catalyst. These results demonstrate that the Al_2O_3 overlayers can stabilize Pd particles under catalytic reaction conditions as harsh as CH_4 combustion. The reference sample, Al_2O_3/SiO_2-T prepared by the ALD method, only showed minor CH_4 conversion above 700 °C (see Figure S13). The catalytic activity of the Pd/SiO_2-T catalysts decreased greatly upon the addition of water to the reactants (see Figure S14), as observed with previously reported supported Pd catalysts,[15] whereas the Al_2O_3 overlayers enhanced the resistance of Al_2O_3/Pd/SiO_2-T catalysts to water (see Figure S15).

The used catalysts were characterized in detail. TEM images (see Figure S8) showed that the Pd particles in the fresh and used Pd/SiO_2-T catalysts had similar size distributions, since the fresh Pd/SiO_2-T catalysts were subjected to calcination at 900 °C in 10% O_2/Ar for 6 h. As shown in Figure 2, the used Pd/SiO_2-T catalysts exhibited predominantly the XRD pattern arising from PdO, the Pd $3d_{5/2}$ binding energy of bulk PdO at 337.1 eV,[11b] and no vibrational feature of adsorbed CO. All these observations demonstrate that the used Pd/SiO_2-T catalysts exhibit the pure PdO phase. However, the used Al_2O_3/Pd/SiO_2-T catalysts exhibited XRD patterns arising from both PdO and Pd phases, the Pd $3d_{5/2}$ binding energies of major PdO_x species at 336.8 eV and minor metallic Pd species at 335.3 eV, and very weak but distinguishable vibrational bands at 2039/2020 cm^{-1} corresponding to CO adsorbed at Pd sites of Pd–PdO_x interfaces. Thus, the used Al_2O_3/Pd/SiO_2-T catalysts should exhibit core–shell-like Pd@(dominant PdO_x + minor Pd) structures. These results demonstrate that the Al_2O_3 overlayers can effectively stabilize the surface PdO_x species on Pd particles in the catalysts under the conditions of CH_4 combustion reactions.

Therefore, Al_2O_3 overlayers on Pd particles coated by ALD not only effectively prevent Pd particles from sintering, but also effectively stabilize the surface PdO_x species. It is well-established that oxidized Pd species dominate at low temperatures and metallic Pd species dominate at high temperatures during the CH_4 combustion reaction. The catalytic activity of various Pd structures in the CH_4 combustion reaction decreases in the order: Pd^0–PdO_x interface > PdO_x species > bulk PdO > Pd^0.[3a,b] Thus, the stability of various Pd species and the Pd speciation under the conditions of the CH_4 combustion reaction govern the catalytic performance of supported Pd catalysts. Fresh Pd/SiO_2-T catalysts are reconstructed into PdO/SiO_2 catalysts after the first cycle of activity evaluation, resulting in an activity decrease in the subsequent cycles of activity evaluation, although the sizes do not vary much. At high temperatures, the reconstruction of fresh Pd/SiO_2-T catalysts from active Pd–PdO_x and PdO_x structures to less active Pd^0 during the heating ramp and the reverse reoxidation and the reverse reconstruction during the cooling ramp result in the observed serious deactivation during the cooling ramp. The stabilization effect of Al_2O_3 overlayers on the surface PdO_x species in Al_2O_3/Pd/SiO_2 catalysts during CH_4 combustion reactions prevents the formation of less active bulk PdO phase at low temperatures, and also retains the active PdO_x and Pd–PdO_x structures at high temperatures, thus greatly enhancing the stability of Al_2O_3/Pd/SiO_2 catalysts in catalyzing CH_4 com-

bustion reactions in a wide temperature range between 200 and 850 °C.

Pd/SiO_2-T and $Al_2O_3/Pd/SiO_2$-T catalysts pretreated under a flow of 10% O_2/Ar at 50 mL min^{-1} for 1 h at 500 °C and then cooled to 200 °C, respectively of bulk PdO and core–shell-like Pd@(dominant PdO_x + minor Pd) structures, were subjected to TPO measurements (Figure 4). Pd/SiO_2-T catalysts exhibited two O_2-production peaks at approximately 780 and 848 °C with comparable intensities during the heating

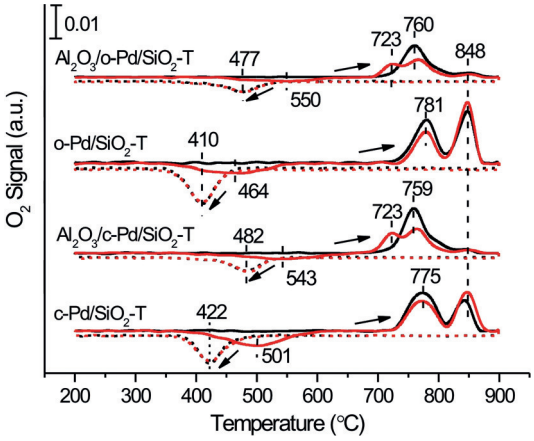

Figure 4. TPO profiles of c-Pd/SiO_2-T, Al_2O_3/c-Pd/SiO_2-T, o-Pd/SiO_2-T, and Al_2O_3/o-Pd/SiO_2-T samples during two cycles (1st cycle: black; 2nd cycle: red) of the heating ramp (solid line) and cooling ramp (dashed line) under 10% O_2/Ar.

ramp, corresponding to the surface decomposition and partial subsurface/bulk decomposition of bulk PdO, and an O_2-consumption peak at approximately 422 °C during the cooling ramp corresponding to the oxidation of the Pd shell on the PdO core. $Al_2O_3/Pd/SiO_2$-T catalysts exhibited a major O_2-production peak at approximately 760 °C and a minor peak at 848 °C during the heating ramp, corresponding to the decomposition of major surface PdO_x species and the minor subsurface PdO phase of the Pd@(dominant PdO_x + minor Pd) structure, respectively, and an O_2-consumption peak at approximately 482 °C during the cooling ramp corresponding to the surface oxidation of Pd particles. The higher reoxidation temperatures also confirm a promoting effect of Al_2O_3 overlayers on Pd reoxidation.

In the subsequent second heating-ramp cycle, a weak and broad O_2-consumption peak emerged for all the catalysts, corresponding to the further reoxidation of multidomain Pd particles in contact with the support.[16] Such further reoxidation processes of $Al_2O_3/Pd/SiO_2$-T catalysts occur at much higher temperatures and with much weaker intensities than for Pd/SiO_2-T catalysts, thus suggesting the less extensive and more difficult oxidation of $Al_2O_3/Pd/SiO_2$-T catalysts with the Pd@(dominant PdO_x + minor Pd) structure. A new O_2-production peak at 723 °C appeared at the expense of the original decomposition peak at 760 °C for $Al_2O_3/Pd/SiO_2$-T catalysts, and is possibly associated with the decomposition of an intermediate of the PdO_x species,[16a,c] whereas the decomposition peak at 848 °C did not vary. Pd/SiO_2-T catalysts exhibited a slightly increased subsurface/bulk decomposition peak at 848 °C at the expense of the surface decomposition peak at approximately 780 °C. In the following cooling cycle, the behavior of all catalysts was similar to that in the first cycle. The TPO profiles of all catalysts remained stable after the second cycle (see Figure S16 and Table S4). These TPO observations suggest a reversible Pd@(dominant PdO_x + minor Pd)↔Pd^0 transformation of $Al_2O_3/Pd/SiO_2$-T catalysts during the CH_4 combustion reaction, but a reversible PdO↔PdO@Pd^0 transformation of Pd/SiO_2-T catalysts. Consequently, $Al_2O_3/Pd/SiO_2$-T catalysts can exhibit active and stable PdO_x and Pd–PdO_x structures during CH_4 combustion up to 850 °C.

High-resolution ^{27}Al magic angle spinning (MAS) NMR spectra of Al_2O_3/c-Pd/SiO_2 and Al_2O_3/c-Pd/SiO_2-T catalysts were measured to study the structures of coated Al_2O_3 overlayers on Pd particles (Figure 5; see also Figure S17). The spectra of reference samples Al_2O_3/SiO_2 and Al_2O_3/SiO_2-T were also measured (see Figure S17). Three peaks with

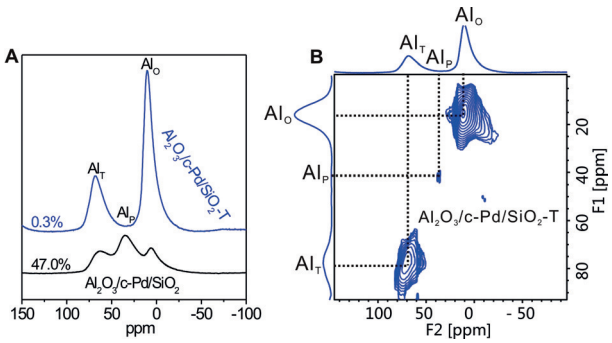

Figure 5. ^{27}Al MAS NMR spectra of A) Al_2O_3/c-Pd/SiO_2 and Al_2O_3/c-Pd/SiO_2-T, and B) corresponding 2D ^{27}Al multiple quantum MAS (MQMAS) NMR spectra for Al_2O_3/c-Pd/SiO_2-T.

chemical shifts centered at 10, 35, and 67 ppm were clearly identified in the spectra of Al_2O_3/c-Pd/SiO_2 and Al_2O_3/SiO_2, and can be assigned to Al^{3+} ions with octahedral (Al_O), pentahedral (Al_P), and tetrahedral (Al_T) coordination environments, respectively.[17a,b] The ^{27}Al MAS NMR spectra were fitted using quadrupolar line shapes with the DMFIT program (see Figure S18 and Table S5).[18] The percentages of Al_P sites are 47.4 and 47.0%, respectively, in Al_2O_3/SiO_2 and Al_2O_3/c-Pd/SiO_2, thus demonstrating the exceptionally high density of Al_P sites on amorphous Al_2O_3 prepared by the ALD method, consistent with previous reports.[17c] The Al_P sites are usually created on γ-Al_2O_3 supports by dehydration and dehydroxylation processes at elevated temperatures with very low densities and exhibit a strong ability to anchor supported metal particles.[17a,b] The percentage of Al_P sites decreased sharply to 0.3% for Al_2O_3/c-Pd/SiO_2-T and only to 18.0% for Al_2O_3/SiO_2-T. Meanwhile, the percentage of Al_O sites increased, whereas that of Al_T sites did not vary much. Thus, a large quantity of Al_P sites should be located at the interfaces of Pd particles and coated Al_2O_3 overlayers in Al_2O_3/c-Pd/SiO_2, and during the subsequent oxidation treatment at 900 °C, these Al_P sites interact with adjacent Pd atoms, most likely induced by surface oxidation of Pd^0 to Pd^{II},

with the formation of Pd^{II}–O–Al bonds and transformation into Al_O sites in Al_2O_3/c-Pd/SiO_2-T. The strong Pd^{II}–O–Al bonds resulting from Al_P sites act to stabilize the surface PdO_x species in Al_2O_3/Pd/SiO_2-T catalysts even during the harsh CH_4 combustion reaction. High-temperature calcination treatment is always involved in the ALD preparation of Al_2O_3-coated metal particles, and its role is assumed only to create pores within the Al_2O_3 overlayers.[7] Our results reveal the hidden key role of high-temperature calcination in creating the strong interaction between metal and Al_P sites to stabilize metal particles. Although Al_2O_3 overlayers on metal particles coated by the ALD method have been frequently reported to stabilize the metal particles, our results clarify the origin of this effect as the presence of abundant Al_P sites in Al_2O_3 overlayers coated on metal particles by ALD that strongly interact and stabilize the coated metal particles.

In summary, efficient and stable Al_2O_3/Pd/SiO_2 catalysts for catalyzing methane combustion between 200 and 850 °C were successfully prepared by an ALD method. Al_2O_3 overlayers coated on Pd particles have abundant pentacoordinated Al^{3+} sites capable of strongly interacting with adjacent surface PdO_x phases on supported Pd particles and stabilizing active PdO_x and PdO_x–Pd structures. These results reveal the underlying mechanism for the significant stabilizing effect of ALD-coated Al_2O_3 overlayers on metal particles and provide a convenient strategy to explore stable and efficient supported Pd catalysts for methane combustion.

Acknowledgements

This research was financially supported by the National Key R & D Program of the Ministry of Science and Technology of China (2017YFB0602205), the National Natural Science Foundation of China (21525313, 91745202, 21703227), the Chinese Academy of Sciences, and the Changjiang Scholars Program of the Chinese Ministry of Education.

Conflict of interest

The authors declare no conflict of interest.

Keywords: atomic layer deposition · heterogeneous catalysis · oxidation · palladium · reduction

How to cite: *Angew. Chem. Int. Ed.* **2019**, *58*, 12043–12048
Angew. Chem. **2019**, *131*, 12171–12176

[1] a) M. Cargnello, J. J. D. Jaen, J. C. H. Garrido, K. Bakhmutsky, T. Montini, J. J. C. Gamez, R. J. Gorte, P. Fornasiero, *Science* **2012**, *337*, 713–717; b) K. Murata, Y. Mahara, J. Ohyama, Y. Yamamoto, S. Arai, A. Satsuma, *Angew. Chem. Int. Ed.* **2017**, *56*, 15993–15997; *Angew. Chem.* **2017**, *129*, 16209–16213.

[2] a) M. Danielis, S. Colussi, C. de Leitenburg, L. Soler, J. Llorca, A. Trovarelli, *Angew. Chem. Int. Ed.* **2018**, *57*, 10212–10216; *Angew. Chem.* **2018**, *130*, 10369–10373; b) A. Toso, S. Colussi, S. Padigapaty, C. de Leitenburg, A. Trovarelli, *Appl. Catal. B* **2018**, *230*, 237–245; c) J. J. Willis, A. Gallo, D. Sokaras, H. Aljama, S. H. Nowak, E. D. Goodman, L. H. Wu, C. J. Tassone, T. F. Jaramillo, F. Abild-Pedersen, M. Cargnello, *ACS Catal.* **2017**, *7*, 7810–7821.

[3] a) N. M. Kinnunen, J. T. Hirvi, M. Suvanto, T. A. Pakkanen, *J. Phys. Chem. C* **2011**, *115*, 19197–19202; b) N. M. Kinnunen, J. T. Hirvi, T. Venäläinen, M. Suvanto, T. A. Pakkanen, *Appl. Catal. A* **2011**, *397*, 54–61; c) X. H. Chen, Y. Zheng, F. Huang, Y. H. Xiao, G. H. Cai, Y. C. Zhang, Y. Zheng, L. L. Jiang, *ACS Catal.* **2018**, *8*, 11016–11028.

[4] a) H. F. Xiong, K. Lester, T. Ressler, R. Schlögl, L. F. Allard, A. K. Datye, *Catal. Lett.* **2017**, *147*, 1095–1103; b) S. K. Matam, M. H. Aguirre, A. Weidenkaff, D. Ferri, *J. Phys. Chem. C* **2010**, *114*, 9439–9443; c) J. D. Grunwaldt, N. van Vegten, A. Baiker, *Chem. Commun.* **2007**, 4635–4637.

[5] a) X. L. Feng, W. Li, D. P. Liu, Z. Zhang, Y. Duan, Y. Zhang, *Small* **2017**, *13*, 1700941; b) M. Monai, T. Montini, C. Chen, E. Fonda, R. J. Gorte, P. Fornasiero, *ChemCatChem* **2015**, *7*, 2038–2046; c) L. Adijanto, D. A. Bennett, C. Chen, A. S. Yu, M. Cargnello, P. Fornasiero, R. J. Gorte, J. M. Vohs, *Nano Lett.* **2013**, *13*, 2252–2257.

[6] a) C. Chen, Y. H. Yeh, M. Cargnello, C. B. Murray, P. Fornasiero, R. J. Gorte, *ACS Catal.* **2014**, *4*, 3902–3909; b) T. M. Onn, S. Y. Zhang, L. Arroyo-Ramirez, Y.-C. Chung, G. W. Graham, X. Q. Pan, R. J. Gorte, *ACS Catal.* **2015**, *5*, 5696–5701.

[7] a) S. M. George, *Chem. Rev.* **2010**, *110*, 111–131; b) J. L. Lu, B. S. Fu, M. C. Kung, G. M. Xiao, J. W. Elam, H. H. Kung, P. C. Stair, *Science* **2012**, *335*, 1205–1208.

[8] M. S. Jin, H. Y. Liu, H. Zhang, Z. X. Xie, J. Y. Liu, Y. N. Xia, *Nano Res.* **2011**, *4*, 83–91.

[9] a) R. L. Puurunen, *J. Appl. Phys.* **2005**, *97*, 121301–121352; b) A. W. Ott, J. W. Klaus, J. M. Johnson, S. M. George, *Thin Solid Films* **1997**, *292*, 135–144; c) J. W. Elam, M. D. Groner, S. M. George, *Rev. Sci. Instrum.* **2002**, *73*, 2981–2987; d) M. D. Groner, F. H. Fabreguette, J. W. Elam, S. M. George, *Chem. Mater.* **2004**, *16*, 639–645.

[10] a) J. A. McCormick, K. P. Rice, D. F. Paul, A. W. Weimer, S. M. George, *Chem. Vap. Deposition* **2007**, *13*, 491–498; b) J. D. Ferguson, A. W. Weimer, S. M. George, *Thin Solid Films* **2000**, *371*, 95–104; c) J. L. Lu, B. Liu, J. P. Greeley, Z. X. Feng, J. A. Libera, Y. Lei, M. J. Bedzyk, P. C. Stair, J. W. Elam, *Chem. Mater.* **2012**, *24*, 2047–2055.

[11] a) J. F. Moulder, W. F. Stickle, P. E. Sobol, K. D. Bomben, *Handbook of X-Ray Photoelectron Spectroscopy*, Physical Electronics, Inc., Eden Prairie, MN, **1995**, p. 119; b) D. N. Gao, C. X. Zhang, S. Wang, Z. S. Yuan, S. D. Wang, *Catal. Commun.* **2008**, *9*, 2583–2587.

[12] a) E. Ozensoy, D. C. Meier, D. W. Goodman, *J. Phys. Chem. B* **2002**, *106*, 9367–9371; b) L. B. Ding, H. Yi, W. H. Zhang, R. You, T. Cao, J. L. Yang, J. L. Lu, W. X. Huang, *ACS Catal.* **2016**, *6*, 3700–3707; c) B. Bourguignon, S. Carrez, B. Dragnea, H. Dubost, *Surf. Sci.* **1998**, *418*, 171–180; d) T. Lear, R. Marshall, J. A. Lopez-Sanchez, S. D. Jackson, T. M. Klapötke, M. Bäumer, G. Rupprechter, H. J. Freund, D. Lennon, *J. Chem. Phys.* **2005**, *123*, 174706; e) M. Peter, J. M. Florescamacho, S. Adamovski, L. K. Ono, K. H. Dostert, C. P. O'Brien, B. Roldancuenya, S. Schauermann, H. J. Freund, *Angew. Chem. Int. Ed.* **2013**, *52*, 5175–5179; *Angew. Chem.* **2013**, *125*, 5282–5287; f) K. Wolter, O. Seiferth, H. Kuhlenbeck, M. Baumer, H. J. Freund, *Surf. Sci.* **1998**, *399*, 190–198; g) H. Feng, J. L. Lu, P. C. Stair, J. W. Elam, *Catal. Lett.* **2011**, *141*, 512–517; h) G. Tofighi, X. J. Yu, H. Lichtenberg, D. E. Doronkin, W. Wang, C. Wöll, Y. M. Wang, J. Grunwaldt, *ACS Catal.* **2019**, *9*, 5462–5473.

[13] a) H. Z. Bao, W. H. Zhang, Q. Hua, Z. Q. Jiang, J. L. Yang, W. X. Huang, *Angew. Chem. Int. Ed.* **2011**, *50*, 12294–12298; *Angew. Chem.* **2011**, *123*, 12502–12506; b) Z. H. Zhang, S. S. Wang, R. Song, T. Cao, L. F. Luo, X. Y. Chen, Y. X. Gao, J. Q. Lu, W. X. Li, W. X. Huang, *Nat. Commun.* **2017**, *8*, 488; c) M. Yang, J. Z. Zhang, Y. Y. Cao, M. F. Wu, K. Qian, Z. H. Zhang, H. Y. Liu,

J. G. Wang, W. Chen, W. X. Huang, *ChemCatChem* **2018**, *10*, 5128 – 5134; d) Z. H. Zhang, H. Wu, Z. Y. Yu, R. Song, K. Qian, X. Y. Chen, J. Tian, W. H. Zhang, W. X. Huang, *Angew. Chem. Int. Ed.* **2019**, *58*, 4276 – 4280; *Angew. Chem.* **2019**, *131*, 4320 – 4324.

[14] a) A. Bensalem, D. Tessier, F. Bozon-Verduraz, *J. Soc. Alg. Chim.* **1993**, *2*, 329; b) A. Bensalem, J. C. Muller, D. Tessier, F. Bozon-Verduraz, *J. Chem. Soc. Faraday Trans.* **1996**, *92*, 3233 – 3237; c) M. Skotak, Z. Karpiński, W. Juszczyk, J. Pielaszek, L. Kępiński, D. V. Kazachkin, V. I. Kovalchuk, J. L. d'Itri, *J. Catal.* **2004**, *227*, 11 – 25; d) D. Tessier, A. Rakai, F. Bozon-Verduraz, *J. Chem. Soc. Faraday Trans.* **1992**, *88*, 741 – 749.

[15] a) R. Kikuchi, S. Maeda, K. Sasaki, S. Wennerström, K. Eguchi, *Appl. Catal. A* **2002**, *232*, 23 – 28; b) R. Butch, F. J. Urbano, P. K. Loader, *Appl. Catal. A* **1995**, *123*, 173 – 184; c) O. Mihai, G. Smedler, U. Nylén, M. Olofssond, L. Olsson, *Catal. Sci. Technol.* **2017**, *7*, 3084 – 3096; d) R. Gholami, M. Alyani, K. J. Smith, *Catalysts* **2015**, *5*, 561 – 594.

[16] a) S. Colussi, A. Trovarelli, G. Groppi, J. Llorca, *Catal. Commun.* **2007**, *8*, 1263 – 1266; b) P. Castellazzi, G. Groppi, P. Forzatti, *Appl. Catal. B* **2010**, *95*, 303 – 311; c) G. Groppi, C. Cristiani, L. Lietti, *Stud. Surf. Sci. Catal.* **2000**, *130*, 3801 – 3806.

[17] a) J. H. Kwak, J. Z. Hu, D. H. Kim, J. Szanyi, C. H. F. Peden, *J. Catal.* **2007**, *251*, 189 – 194; b) J. H. Kwak, J. Z. Hu, D. H. Mei, C. W. Yi, D. H. Kim, C. H. F. Peden, L. F. Allard, J. Szanyi, *Science* **2009**, *325*, 1670 – 1673; c) K. L. Sung, Y. P. Sun, S. Y. Yoo, M. Jaehyun, *J. Phys. Chem. C* **2010**, *114*, 13890 – 13894; d) L. Baggetto, V. Sarou-Kanian, P. Florian, A. N. Gleizes, D. Massiot, C. Vahlas, *Phys. Chem. Chem. Phys.* **2017**, *19*, 8101 – 8110; e) V. Sarou-Kanian, A. N. Gleizes, P. Florian, D. Samelor, D. Massiot, C. Vahlas, *J. Phys. Chem. C* **2013**, *117*, 21965 – 21971.

[18] a) J. Z. Hu, S. C. Xu, J. H. Kwak, M. Y. Hu, C. Wan, Z. C. Zhao, J. Szanyi, X. H. Bao, X. W. Han, Y. Wang, C. H. F. Peden, *J. Catal.* **2016**, *336*, 85 – 93; b) D. Massiot, F. Fayon, M. Capron, I. King, S. L. Calvé, B. Alonso, J. O. Durand, B. Bujoli, Z. H. Gan, G. Hoatson, *Magn. Reson. Chem.* **2002**, *40*, 70 – 76; c) Z. C. Zhao, S. C. Xu, M. Y. Hu, X. H. Bao, C. H. F. Peden, J. Z. Hu, *J. Phys. Chem. C* **2015**, *119*, 1410 – 1417.

Manuscript received: April 19, 2019
Accepted manuscript online: June 13, 2019
Version of record online: July 24, 2019

